N-glycosylation–dependent regulation of hK$_{2P}$17.1 currents

Felix Wiedmann[a,b,c]**, Daniel Schlund**[a]**, Niels Voigt**[d,e]**, Antonius Ratte**[a,b,c]**, Manuel Kraft**[a,b,c]**,
Hugo A. Katus**[a,b,c]**, and Constanze Schmidt**[a,b,c,*]

[a]Department of Cardiology, [b]DZHK (German Center for Cardiovascular Research), Partner Site Heidelberg/Mannheim,
and [c]HCR, Heidelberg Center for Heart Rhythm Disorders, University of Heidelberg, 69120 Heidelberg, Germany;
[d]Institute of Pharmacology and Toxicology, University Medical Center Göttingen, Georg-August University of
Göttingen, 37073 Göttingen, Germany; [e]DZHK (German Center for Cardiovascular Research), Partner Site Göttingen,
University of Göttingen, 37073 Göttingen, Germany

ABSTRACT Two pore-domain potassium (K$_{2P}$) channels mediate potassium background currents that stabilize the resting membrane potential and facilitate action potential repolarization. In the human heart, hK$_{2P}$17.1 channels are predominantly expressed in the atria and Purkinje cells. Reduced atrial hK$_{2P}$17.1 protein levels were described in patients with atrial fibrillation or heart failure. Genetic alterations in hK$_{2P}$17.1 were associated with cardiac conduction disorders. Little is known about posttranslational modifications of hK$_{2P}$17.1. Here, we characterized glycosylation of hK$_{2P}$17.1 and investigated how glycosylation alters its surface expression and activity. Wild-type hK$_{2P}$17.1 channels and channels lacking specific glycosylation sites were expressed in *Xenopus laevis* oocytes, HEK-293T cells, and HeLa cells. N-glycosylation was disrupted using N-glycosidase F and tunicamycin. hK$_{2P}$17.1 expression and activity were assessed using immunoblot analysis and a two-electrode voltage clamp technique. Channel subunits of hK$_{2P}$17.1 harbor two functional N-glycosylation sites at positions N65 and N94. In hemi-glycosylated hK$_{2P}$17.1 channels, functionality and membrane trafficking remain preserved. Disruption of both N-glycosylation sites results in loss of hK$_{2P}$17.1 currents, presumably caused by impaired surface expression. This study confirms diglycosylation of hK$_{2P}$17.1 channel subunits and its pivotal role in cell-surface targeting. Our findings underline the functional relevance of N-glycosylation in biogenesis and membrane trafficking of ion channels.

INTRODUCTION

Two pore-domain (K$_{2P}$) potassium channels mediate background potassium leak currents that stabilize the resting membrane potential and control cellular excitation by shaping the duration, frequency, and amplitude of action potentials (Ketchum *et al.*, 1995; Goldstein *et al.*, 2001).

The alkaline-activated K$_{2P}$-channels human (h)K$_{2P}$5.1 (TWIK-related acid-sensing K$^+$ channel [TASK]-2), hK$_{2P}$16.1 (TWIK-related alkaline-pH–activated K$^+$ channel [TALK]-1) and hK$_{2P}$17.1 (TWIK-related alkaline-pH–activated K$^+$ channel [TALK]-2) display strong expression in the pancreas and were assumed to be involved in

FIGURE 1: Putative N-glycosylation sites of hK$_{2P}$17.1. (A) Schematic two-dimensional membrane model of an hK$_{2P}$17.1 subunit. Putative N-glycosylated asparagine residues 65 and 94 in the M1-P1 linker are highlighted. P, pore-forming domain; M, transmembrane domain; N, N-terminus; C, C-terminus; extracellular site top, intracellular site bottom. (B) Three-dimensional homology model of hK$_{2P}$17.1, assembled as dimer illustrates that asparagine residues 65 and 94 are directed toward the extracellular site and therefore accessible to N-glycosylation. (C) Species conservation of N-glycosylation motives at asparagine residues 65 and 94. *, full conservation; :, conservative substitution; ., semi-conservative substitution.

bicarbonate secretion (Enyedi and Czirják, 2010; Feliciangeli *et al.*, 2015). In addition, hK$_{2P}$17.1 mRNA is expressed in the liver, lung, and brain (Decher *et al.*, 2001). In the human heart, hK$_{2P}$17.1 channels are predominantly expressed in the atria and the Purkinje system of the ventricles (Decher *et al.*, 2001; Friedrich *et al.*, 2014; Schmidt *et al.*, 2015).

Atrial expression of hK$_{2P}$17.1 is reduced in patients with atrial fibrillation (AF) and heart failure (HF) (Schmidt *et al.*, 2015, 2017). The association between a genetic hK$_{2P}$17.1 variant and ischemic stroke further indicates that hK$_{2P}$17.1 channels might be involved in the pathophysiology of AF (Domingues-Montanari *et al.*, 2010; Ma *et al.*, 2013; He *et al.*, 2014). Recently, genetic alterations in hK$_{2P}$17.1 channels have been linked to cardiac conduction disorders (Friedrich *et al.*, 2014; Chai *et al.*, 2018).

Increasing evidence suggests that hK$_{2P}$17.1 channels are important contributors to cardiac electrophysiology (Wiedmann *et al.*, 2016), but little is known about specific mechanisms regulating hK$_{2P}$17.1 expression and cellular trafficking and function. Glycosylation is known to play a crucial role in biosynthesis, transport, and function of transmembrane proteins. Addition and processing of asparagine-linked (N-linked) oligosaccharides is the most common form of glycosylation (Ohtsubo and Marth, 2006). As with most transmembrane proteins, several ion channels undergo posttranslational modifications by N-glycosylation, which influences cellular trafficking, gating, and recycling (Khanna *et al.*, 2001; Baycin-Hizal *et al.*, 2014). The present study was initiated to evaluate whether hK$_{2P}$17.1 channels undergo N-glycosylation, and how glycosylation of hK$_{2P}$17.1 channels may alter their abundance, transport to the plasma membrane, surface expression, and activity.

RESULTS

To select glycosylation sites in hK$_{2P}$17.1 channels that might be physiologically relevant, we applied the bioinformatic software NetNGlyc 1.0 server. The software suggested asparagine residues 65 and 94 as potential N-glycan acceptors with probability scores of 0.72 and 0.73. Both motives are localized in the extracellular M1-P1 interdomain of the hK$_{2P}$17.1 monomer (Figure 1A) and display strong conservation among K$_{2P}$17.1 homologues from different species (Figure 1B). We systematically characterized the predicted glycosylation sites using molecular biological and electrophysiological techniques.

Immunodetection of glycosylated and nonglycosylated channels

To characterize N-glycosylation of hK$_{2P}$17.1 channels, epitope-tagged channel subunits were heterologously expressed in *Xenopus laevis* oocytes. Oocytes expressing hK$_{2P}$17.1 were treated with N-glycosidase F (PNGase F) to cleave oligosaccharides from proteins and hydrolyze asparagine residues to aspartic acid (Tarentino *et al.*, 1985). Immunoblotting revealed that the molecular weight of the hK$_{2P}$17.1 subunit decreased after PNGase F treatment. After deglycosylation, the band for hK$_{2P}$17.1 that was originally located at 35.9 ± 0.3 kDa separated into two bands at 33.0 ± 0.3 and 31.3 ± 0.2 kDa (Figure 2A). Similar mobility shifts of hK$_{2P}$17.1 monomers were observed in hK$_{2P}$17.1-expressing oocytes cultured in the presence of 2 ng/μl tunicamycin, an antibiotic in vivo inhibitor of N-glycosylation (Kuo and Lampen, 1974; Egenberger *et al.*, 2010). We concluded that the three bands represent fully diglycosylated, monoglycosylated, and nonglycosylated hK$_{2P}$17.1 monomers.

FIGURE 2: N-glycosylation regulates current amplitude of hK$_{2P}$17.1 channels expressed in *Xenopus* oocytes. (A) Immunoblot of *Xenopus* oocyte lysates heterologously expressing hK$_{2P}$17.1-myc proteins under control conditions, in the presence of the N-glycosylation inhibitor tunicamycin or after cleavage of N-linked sugar moieties with PNGase F. Glyceraldehyde-3-phosphate dehydrogenase (GAPDH) served as loading control. Insert: schematic illustration of C-terminal myc-tagged hK$_{2P}$17.1 subunits. (B) Dose–response curve of tunicamycin on outward potassium currents of *Xenopus* oocytes, heterologously expressing hK$_{2P}$17.1 channels, 24 h after cRNA injection ($n = 5$–8). (C) Time course of tunicamycin-induced inhibition of hK$_{2P}$17.1 currents, expressed in *Xenopus* oocytes. Measurements were performed 48 h after cRNA injection. Different time intervals of tunicamycin incubation (as provided) refer to time intervals directly before the measurement (i.e., 2 h of tunicamycin incubations means the start of the incubation period is 46 h after injection and TEVC measurements were carried out 48 h postinjection; $n = 10$–12). (D) Resting membrane potential (RMP) of uninjected *Xenopus* oocyte and cells expressing hK$_{2P}$17.1 are depicted under control conditions (clear bars) and after 48 h of incubation with 2 µg/ml tunicamycin (black bars). (E) Families of hK$_{2P}$17.1 current traces after 48 h of incubation with 2 µg/ml tunicamycin or after 48 h of incubation in the respective amount of DMSO (CTRL). (F) Corresponding mean step current amplitudes of the currents displayed in E are plotted as functions of test pulse potentials. (G) Upon 24 h of incubation with tunicamycin (TM), reversibility was probed by incubation in tunicamycin-free medium for another 24 h. Data are given as mean values ± SEM; pulse protocols and scale bars as well as *p* values of two-tailed Student's *t* tests (vs. respective CTRL) are indicated above or below the bars.

Functional implications of hK$_{2P}$17.1 glycosylation

To further assess the functional relevance of N-glycosylation, *X. laevis* oocytes expressing hK$_{2P}$17.1 channels were investigated using the two-electrode voltage clamp technique. HK$_{2P}$17.1-mediated currents were elicited by a voltage step from –80 to +20 mV (500 ms), applied at a frequency of 0.2 Hz. Figure 2B visualized the concentration-dependent inhibitory effect of different tunicamycin concentrations on hK$_{2P}$17.1 currents. Immediately after cRNA injection, oocytes were transferred to media containing the indicated amounts of tunicamycin. Measurements were performed 24 h after injection. Cells incubated in media containing equal amounts of the vehicle dimethyl sulfoxide (DMSO) served as controls. The time course of tunicamycin-induced hK$_{2P}$17.1 current reduction is depicted in Figure 2C. Current recordings were performed 48 h after cRNA injection and cells were incubated in tunicamycin-containing media for the indicated number of hours before current recordings. Therefore, in the 48-h group, tunicamycin was administered immediately after injection and *Xenopus* oocytes displayed mean outward potassium currents of 0.66 ± 0.07 µA, while oocyte currents after control incubation in DMSO reached 1.97 ± 0.28 µA ($p = 0.019$; $n = 10$–12).

After inhibition of hK$_{2P}$17.1 N-glycosylation by tunicamycin for 48 h, *Xenopus* oocytes displayed resting membrane potentials (RMP) of -44.1 ± 1.7 mV, while control cells kept in DMSO-containing media showed an RMP of -50 ± 1.3 mV ($p = 0.14$; $n = 10$–12;

Figure 2D). Uninjected *Xenopus* oocytes displayed RMPs of -29.6 ± 1.5 mV after 48 h of tunicamycin incubation and -26.4 ± 2.2 mV under control conditions ($p = 0.8$; $n = 9$). Representative families of hK$_{2P}$17.1 current traces elicited by the depicted pulse-step protocol from oocytes under control conditions (CTRL) or after incubation with 2 µg/ml tunicamycin for 48 h are visualized in Figure 2E. Corresponding mean step-current amplitudes of these cells, plotted as functions of test pulse potentials are depicted in Figure 2F. To probe reversibility of tunicamycin-induced inhibition of hK$_{2P}$17.1 N-glycosylation, oocytes were either cultured in the absence (w/o TM) or in the presence (w/ TM) of tunicamycin for 48 h after cRNA injection. A third group was kept in tunicamycin for 24 h, followed by incubation in tunicamycin-free medium for another 24 h (Figure 2G). In this group no significant washout of the tunicamycin-induced hK$_{2P}$17.1 current reduction could be observed (48 h tunicamycin: 0.62 ± 0.07 µA, 24 h/24 h: 0.52 ± 0.1 µA; $p = 0.46$; $n = 10$–13).

The route of tunicamycin delivery was not relevant, as intracytoplasmic coninjection of tunicamycin reduced hK$_{2P}$17.1 currents in a similar manner (Supplemental Figure 1).

Expression and functional analysis of hK$_{2P}$17.1 channels lacking glycosylation sites

To evaluate the functional relevance of N-glycosylation sites N65 and N95, two single-channel mutants and one double-mutant
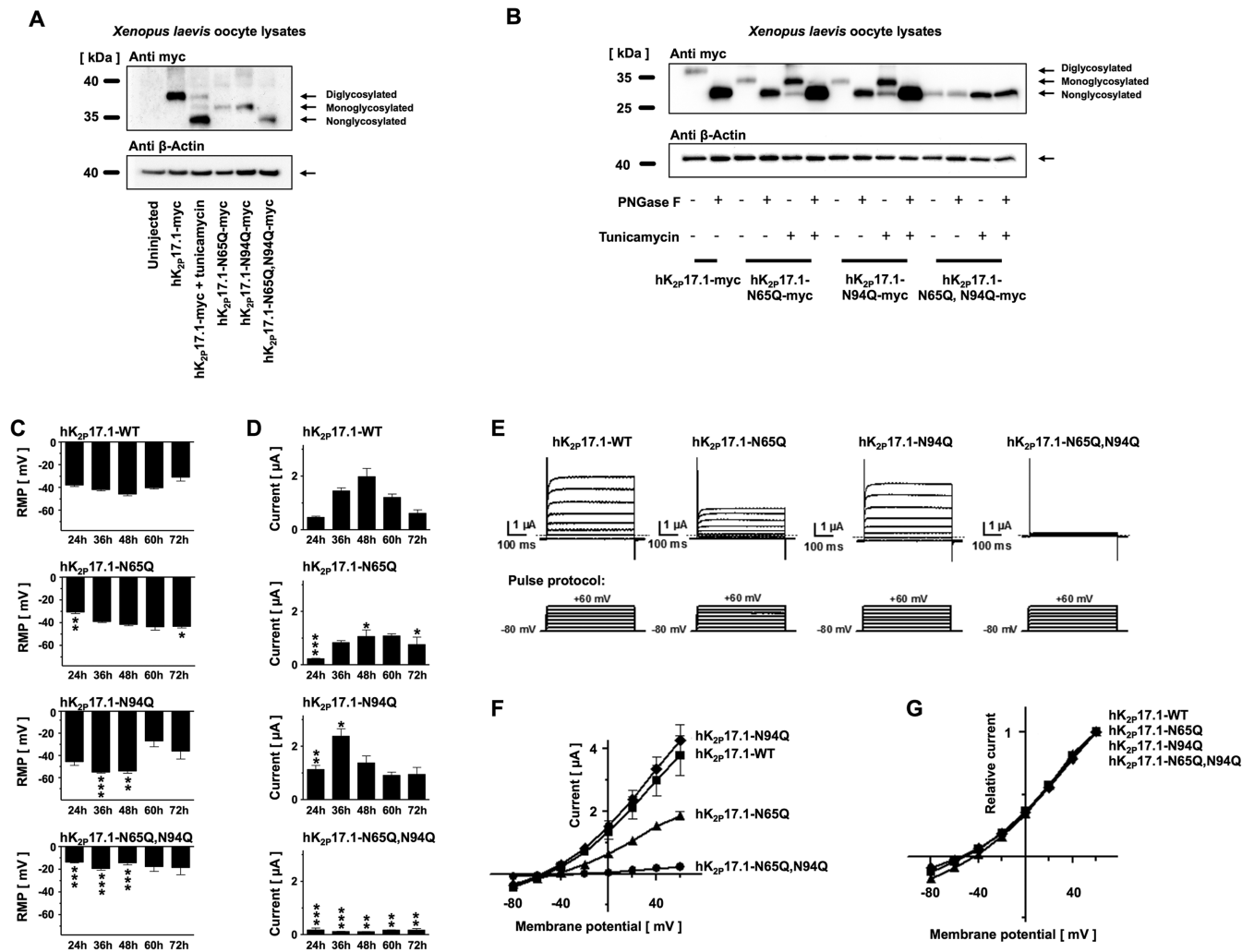
FIGURE 3: Verification of hK$_{2P}$17.1 glycosylation sites. (A) Lysates of *Xenopus* oocytes, expressing the indicated glutamine mutants of hK$_{2P}$17.1-myc, were separated by SDS–PAGE followed by anti-myc immunoblotting. Elimination of N-glycosylation motives resulted in increased protein mobility. Tunicamycin was administered as indicated. β-Actin immunoreactivity served as loading control. (B) Glutamine mutants of hK$_{2P}$17.1-myc, heterologously expressed in *Xenopus* oocytes, were treated with the N-glycosidase PNGase F or the N-glycosylation inhibitor tunicamycin as indicated, followed by SDS–PAGE and anti-myc immunoblotting. β-Actin signals served as loading control. (C, D) *Xenopus* oocytes were injected with cRNA of either WT hK$_{2P}$17.1 or indicated glutamine mutants. Measurements were taken at different time points between 24 and 72 h. (C) Resting membrane potential (RMP) of the cells. (D) Outward potassium currents, measured at the end of a 500-ms +20-mV test pulse (*n* = 4–10). (E) Representative sets of macroscopic potassium current recordings in *Xenopus* oocytes expressing hK$_{2P}$17.1-WT or glutamine mutants. Currents were elicited by application of the test pulse protocol as depicted at the bottom. Dotted lines indicate zero current levels. (F, G) Corresponding mean step current amplitudes are plotted as functions of test pulse potentials to compare mean current–voltage relationships of artificially di-, mono-, and nonglycosylated hK$_{2P}$17.1 monomers. (F) Original current amplitudes. (G) Currents normalized to maximum currents at +60 mV (*n* = 6–9). Data are given as mean values ± SEM. *, $p < 0.05$; **, $p < 0.01$; ***, $p < 0.001$ for Bonferroni-corrected two-tailed Student's *t* tests.

construct were generated. Either one of the asparagine residues 65 and 95 or both residues were mutated to glutamine to prevent carbohydrate modification of these residues. When separated by SDS gel electrophoresis, mutant constructs hK$_{2P}$17.1-N65Q-myc, hK$_{2P}$17.1-N94Q-myc, and hK$_{2P}$17.1-N65Q,N94Q-myc displayed similar mobility shifts, as observed under tunicamycin and glycosidase treatment (Figure 3A).

Deglycosylation by PNGase F or inhibition of N-glycosylation by tunicamycin increased the electrophoretic mobility of the mutant constructs hK$_{2P}$17.1-N65Q-myc and hK$_{2P}$17.1-N94Q-myc to levels similar to those observed for the glutamine double mutant (Figure 3B).

No further change of electrophoretic mobility was observed when the double mutant hK$_{2P}$17.1-N65Q,N94Q-myc was exposed to glycosidase treatment or tunicamycin, which indicates that no further functionally relevant N-glycosylation sites in hK$_{2P}$17.1 monomers exist.

Expressing wild-type hK$_{2P}$17.1 channels as well as single-mutant channels hK$_{2P}$17.1-N65Q and hK$_{2P}$17.1-N94Q in oocytes resulted in a significant reduction of RMP in comparison to uninjected controls (RMP$_{CTRL,t}$ $_{= 24 h}$ = −12.4 ± 0.4 mV; RMP$_{WT,t}$ $_{= 24 h}$ = −37.9 ± 1.4 mV, *n* = 8, $p < 0.0001$; RMP$_{N65Q, t}$ $_{= 24 h}$ = −30.6 ± 1.5 mV, *n* = 8, $p < 0.0001$; RMP$_{N94Q, t}$ $_{= 24 h}$ = −45.4 ± 3.5 mV, *n* = 8, $p < 0.0001$). Expressing double-mutant hK$_{2P}$17.1-N65Q,N94Q channels in oocytes

A hK$_{2P}$17.1-HA-myc
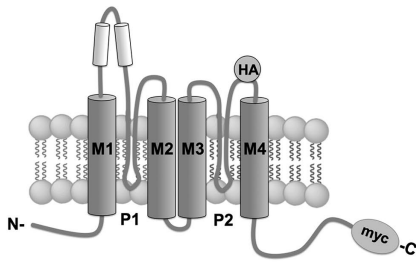
B

Chemiluminescence surface expression assay
Xenopus laevis oocytes
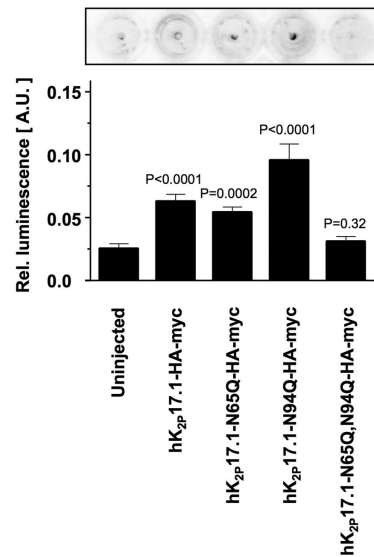
FIGURE 4: N-glycosylation regulates surface expression of hK$_{2P}$17.1. (A) Schematic diagram of the hK$_{2P}$17.1-myc-HA construct used in this experiment. An internal HA tag localized at the extracellular part of the P2-M4 interdomain was used for immunological detection of hK$_{2P}$17.1 dimers at the surface of nonpermeabilized *Xenopus* oocytes. (B) Surface expression of WT hK$_{2P}$17.1 and mutants was measured by HRP-mediated chemiluminescence in *Xenopus* oocytes. Data are given as mean values ± SEM of n = 11– 29 cells, p values are indicated above the bars.

did, however, not affect the RMP (RMP$_{CTRL,t = 24 h}$ = −12.4 ± 0.4 mV; RMP$_{N65Q,N94Q, t = 24 h}$ = −13.7 ± 0.8 mV, n = 8, p = 0.16), suggesting a lack of functional hK$_{2P}$17.1 current.

Intracytoplasmatic injection of hK$_{2P}$17.1-WT cRNA gave rise to noninactivating outward potassium currents. Between 24 and 48 h after injection of cRNA, hK$_{2P}$17.1-WT currents increased from 0.47 ± 0.04 to 2.18 ± 0.3 μA, followed by current reduction to 0.61 ± 0.1 μA between 48 and 72 h (Figure 3, C–G). Injecting oocytes with cRNA for hK$_{2P}$17.1-N65Q channel subunits caused a gradual current increase to 49.7% of the maximum current measured in oocytes expressing WT hK$_{2P}$17.1 at 60 h postinjection. In oocytes expressing hK$_{2P}$17.1-N94Q channel subunits, a maximal current equal to 110.2% of the maximum current measured in oocytes expressing WT channels was observed 36 h postinjection, followed by a gradual current decrease. hK$_{2P}$17.1-N65Q,N94Q ion-channel subunits failed to generate functional currents that differed from those in uninjected oocytes, indicating that the physiological function of the ion channel is lost in the double mutant. Further immunoblots conducted in the presence and absence of DTT demonstrated that K$_{2P}$17.1-N65Q,N94Q double mutant–channel subunits were able to form channel dimers (Supplemental Figure 2). Therefore the observed loss of membrane targeting of nonglycosylated ion channel subunits is not caused by disrupted channel dimerization. To finally exclude mutagenesis-related bias, another set of hK$_{2P}$17.1 mutants was generated. In these mutants, N-glycosylation was disrupted by switching the threonine of the N-(x)-S/T N-glycosylation consensus sequence to alanine (Supplemental Figure 3A). Upon heterologous expression in *Xenopus* oocytes, single-mutant channels showed relevant current expression, while the nonglycosylated double-mutant construct failed to produce measurable potassium currents that differ from those in uninjected *Xenopus* oocytes (Supplemental Figure 3, B–D), similar to the results observed in Figure 3.

As the novel atrial specific antiarrhythmic drug vernakalant was recently characterized as a potent hK$_{2P}$17.1 activator when applied in supratherapeutic concentrations (Seyler *et al.*, 2014) further experiments were conducted to probe whether hK$_{2P}$17.1-N65Q,N94Q currents could be enhanced via application of vernakalant. While hK$_{2P}$17.1-WT, hK$_{2P}$17.1-N65Q, and hK$_{2P}$17.1-N94Q showed strong current activation upon incubation with 100 μM vernakalant for 30 min, hK$_{2P}$17.1-N65Q,N94Q currents did not show any statistically significant alterations (unpublished data).

Surface expression of glycosylated vs. nonglycosylated channels

To determine whether the observed loss of functional potassium currents in nonglycosylated hK$_{2P}$17.1 channels was due to altered channel activity or reduction in cell surface expression, chemoluminescence assays were performed in *X. laevis* oocytes. HK$_{2P}$17.1 surface expression was measured in nonpermeabilized oocytes expressing wild-type or glutamine-mutant constructs that both contained noninterfering HA tags in the extracellular portion of the P2-M4 interdomain. Ion channels present at the cell surface were detected after immunostaining with standardized antibodies (Figure 4A).

Oocytes expressing hK$_{2P}$17.1-N65Q-HA-myc constructs displayed chemiluminescence signals comparable to WT channels (Figure 4B). Channel surface expression of hK$_{2P}$17.1-N94Q-HA-myc cRNA was even higher than that of WT channels (Figure 4B). Double-mutant hK$_{2P}$17.1-N65Q,N94Q-HA-myc constructs, however, displayed chemiluminescence signals virtually indistinguishable from those in uninjected control oocytes, arguing against significant surface expression of these channel subunits. Taken together, these findings indicate that the reduced current of channels lacking both glycosylation sites was caused by loss of membrane recruitment rather than by changes in functionality (Figure 4B).

N-glycosylation of hK$_{2P}$17.1 in mammalian cells

To confirm N-glycosylation of hK$_{2P}$17.1 in mammalian cells and to further exclude interference of the myc affinity tag, native hK$_{2P}$17.1-WT channels were expressed in HEK-293T cells in the presence or absence of tunicamycin and subjected to treatment with PNGase-F. Immunoblotting confirmed the presence of diglycosylated, monoglycosylated, and nonglycosylated channel subunits (Figure 5A). This result could be reproduced by gel electrophoresis and immunoblot of hK$_{2P}$17.1-N65Q, hK$_{2P}$17.1-N94Q, and hK$_{2P}$17.1-N65Q,N94Q mutant ion-channel subunits (Figure 5B). Again, no further mobility shift was observed by exposing hK$_{2P}$17.1-N65Q,N94Q lysates to glycosidase treatment or tunicamycin coincubation, arguing against additional active N-glycosylation sites (Figure 5B). Surface expression of glycosylation-deficient hK$_{2P}$17.1 channel subunits was further detected using surface biotinylation (Figure 5C). Immunodetection after precipitation with avidin-coupled beads confirmed the absence of hK$_{2P}$17.1-N65Q,N94Q double mutants in HEK-239T surface fractions (p < 0.0001, n = 3; Figure 5D), while appropriate
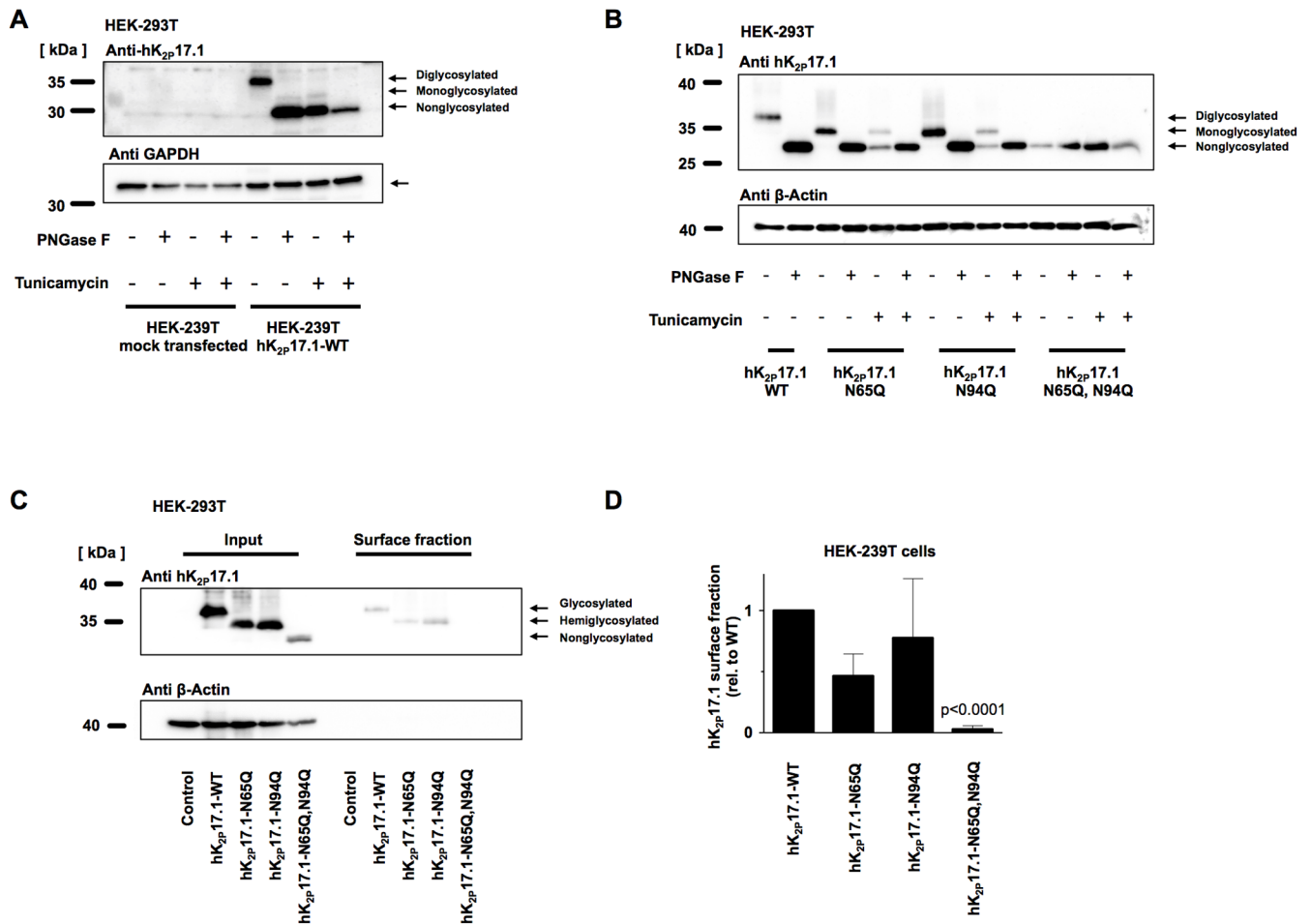
FIGURE 5: N-glycosylation of hK$_{2P}$17.1 expressed in mammalian cells. (A) hK$_{2P}$17.1-WT channel subunits were heterologously expressed in HEK-293T cells in the presence or absence of the N-glycosylation inhibitor tunicamycin. Cell lysates were digested with PNGase F to remove N-linked sugar moieties as indicated. Immunoblots for glyceraldehyde-3-phosphate dehydrogenase (GAPDH) served as loading control. (B) WT hK$_{2P}$17.1 channel subunits and glutamine mutants were expressed in HEK-293T cells and treated as described in A. (C) Surface fractions of HEK-293T cells expressing indicated hK$_{2P}$17.1 variants were isolated by surface biotinylation followed by streptavidin precipitation. (D) Mean optical densities of the surface blots were normalized to the signal of WT hK$_{2P}$17.1. Data are provided as mean values ± SEM of three independent experiments.

membrane trafficking was observed in WT and monoglycosylated hK$_{2P}$17.1. Expression of WT hK$_{2P}$17.1 and glycosylation-deficient mutants in HeLa cells and visualization of membrane trafficking via immunofluorescence again confirmed cell surface expression of hK$_{2P}$17.1-WT, hK$_{2P}$17.1-N65Q, and hK$_{2P}$17.1-N94Q subunits while hK$_{2P}$17.1-N65Q,N94Q double mutants were not present at the plasma membrane (Figure 6).

Effects of external glucose concentration on surface expression of hK$_{2P}$17.1 in HEK-293T cells

To study how external glucose concentration influences hK$_{2P}$17.1 N-glycosylation state and surface expression, HEK-239T cells heterologously expressing hK$_{2P}$17.1-WT channels were cultured and maintained in media with glucose concentrations of 2.1–4.5 g/l. Surface expression of hK$_{2P}$17.1 was assessed after surface protein biotinylation and streptavidin precipitation followed by SDS–PAGE and immunoblot (Figure 7A). While nontransfected cells and biotin-negative controls showed no hK$_{2P}$17.1 protein in surface fractions, cells cultured in 4.5 g/l glucose displayed a robust hK$_{2P}$17.1 surface frac-

tion. With reduction of the extracellular glucose concentration, a gradual decrease of hK$_{2P}$17.1 protein surface expression was observed. No changes were observed, however, in the glycosylation state of hK$_{2P}$17.1 (Figure 7, B–D)

O-glycosylation of hK$_{2P}$17.1 channels

To assess whether hK$_{2P}$17.1 subunits undergo O-glycosylation, lysates of HEK-293T cells expressing hK$_{2P}$17.1 were treated with the O-glycosylation inhibitor benzyl 2-acetamido-2-deoxy-α-D-galactopyranoside. After incubation with neuraminidase, O-glycosidic bonds were digested with O-glycosidase. Essentially, the pattern of hK$_{2P}$17.1 immunoblot bands was not changed after treatment with benzyl 2-acetamido-2-deoxy-α-D-galactopyranoside. After enzymatic deglycosylation with neuraminidase and O-glycosidase, another protein band could be observed (Figure 8, gray arrow). However, this mobility shift could not be reproduced in hK$_{2P}$17.1-N65Q,N94Q double-mutant subunits. Therefore, it is likely that this band resembles modifications of N-linked sugar moieties as a result of the pretreatment with neuraminidase. Taken
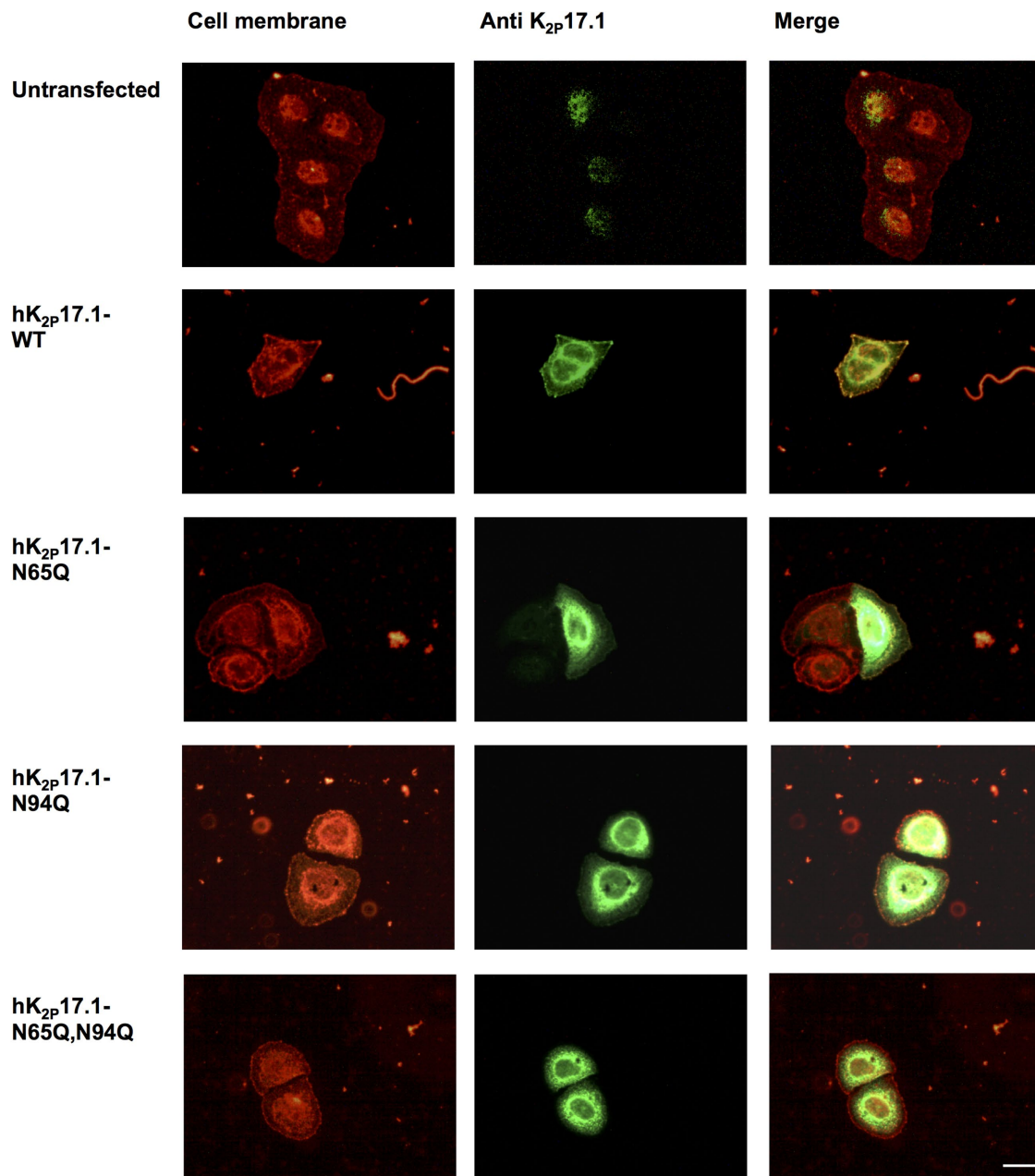
FIGURE 6: N-glycosylation–dependent hK$_{2P}$17.1 surface expression in HeLa cells. WT hK$_{2P}$17.1 or glutamine mutants lacking either one or both N-glycosylation motives were expressed in HeLa cells. Cell membranes stained with Alexa 594-labeled wheat germ agglutinin are depicted in red. Immunostaining of hK$_{2P}$17.1-variants is shown in green. Overlays demonstrate co-localization of di- and monoglycosylated hK$_{2P}$17.1 subunits with the cell membrane. Nonglycosylated double-mutant channels cannot be detected at the cell membrane. Scale bar: 5 µm.

together, these results support the hypothesis that heterologously expressed hK$_{2P}$17.1 ion-channel subunits are not subjected to O-glycosylation.

DISCUSSION

Posttranslational modification by attachment of sugar moieties is a common feature of ion channels because of their role as membrane proteins. In general, posttranslational glycosylation can influence function, folding, solubility, stability, and trafficking of ion-channel proteins. Except for nonfunctional hK$_{2P}$15.1 channels, all members of the two pore–domain potassium channel family harbor one or two putative N-glycosylation sites in the M1-P1 interdomain (Mant *et al.*, 2013). It was, however, shown that not all predicted N-glycosylation sites undergo glycan modification. Egenberger *et al.* (2010) reported that only one of the two putative N-glycosylation sites of K$_{2P}$18.1 (TRESK, TWIK-related spinal cord K$^+$ channel) is glycosylated. Therefore, it is necessary to confirm predicted glycosylation sites experimentally to fully characterize the molecular function of ion channels. Crystal structures of the ion channel proteins hK$_{2P}$1.1, hK$_{2P}$2.1, hK$_{2P}$4.1, and hK$_{2P}$10.1 were determined only for synthetic constructs, in which potential glycosylation sites were removed (Brohawn *et al.*, 2012; Miller and Long, 2012). Therefore, available crystallographic structures do not contain information about K$_{2P}$-channel glycosylation. To our knowledge, our study is the
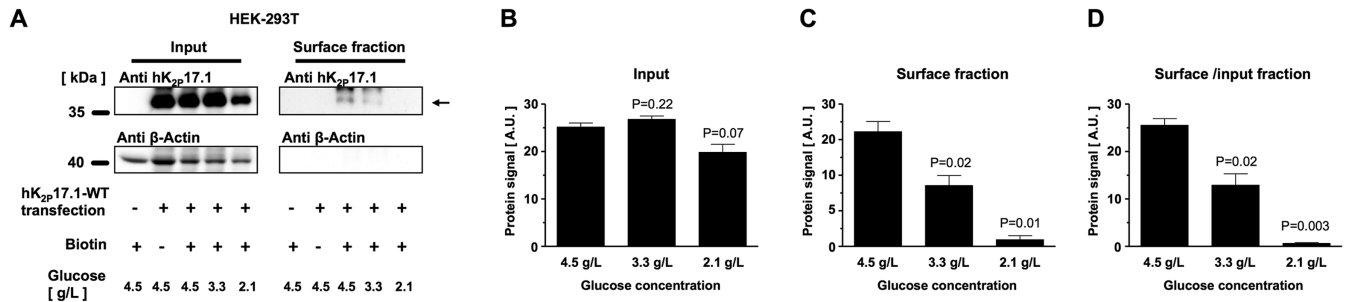
FIGURE 7: Effects of external glucose concentration on surface expression of hK$_{2P}$17.1 in HEK-293T cells. (A) Representative immunoblots of hK$_{2P}$17.1-WT channels expressed in HEK-293T cells cultured under different glucose concentrations. Input fractions (left) are provided, as well as surface fractions (right) obtained via surface biotinylation and streptavidin precipitation. Transfection state, absence or presence of biotin, and external glucose concentration are displayed. (B) Mean hK$_{2P}$17.1 protein signals in the input fractions of $n = 3$ independent experiments, quantified via densitometry. (C) Mean optical densities of hK$_{2P}$17.1 protein signals in the respective surface fractions. (D) Ratio of hK$_{2P}$17.1 protein signals of surface/input fractions. Data are presented as mean ± SEM. p values of two-tailed Student's t tests vs. glucose 4.5 g/l are given as inserts.

first to show the importance of hK$_{2P}$17.1-channel glycosylation for its localization and function. Combining experimental techniques to characterize pharmacological, molecular, and electrophysiological properties of hK$_{2P}$17.1, we show that subunits of this ion channel harbor two functionally active N-glycosylation sites at positions N65 and N94. Mutant channel subunits containing only one N-glycosylation site are still recruited to the plasma membrane, and potassium outward currents are detectable in oocytes expressing these mutants. Abrogation of both N-glycosylation sites, however, appears to abolish the function of hK$_{2P}$17.1 completely due to impaired transport to the cell surface. Loss of membrane targeting of nonglycosylated ion-channel subunits is not caused by disrupted channel dimerization as described for other glycosylated proteins (He *et al.*, 2002).

Interestingly, inactivating glycosylation at N65 results in prolonged membrane currents, which indicates an increased residence time at the plasma membrane relative to WT channels or channel mutants deficient in glycosylation at N94 (Figure 3, C and D). It might therefore be speculated that N65-linked sugar moieties influ-

ence the internalization or recycling of hK$_{2P}$17.1 subunits. When protein expression levels of the hK$_{2P}$17.1-N65Q,N94Q double mutant are compared with those of single-mutant or wild-type channels, it is striking that expression of double mutant–channel subunits is much higher in HEK-293T cell lysates than in *X. laevis* oocytes. This could, at least in part, be explained by better expression of human K$_{2P}$17.1 channel isoforms in the mammalian cellular context or by different degradation mechanisms of nonfunctional proteins. Surface expression of hK$_{2P}$17.1-N65Q,N94Q double mutant–channel subunits was, however, disrupted in both *Xenopus* oocytes and mammalian cells.

It was previously shown that inhibition of N-linked glycosylation alters the voltage dependency of ion-channel gating in Kv1.1 and KvLQT1 channels (Thornhill *et al.*, 1996; Freeman *et al.*, 2000). However, voltage dependency remains unchanged in hK$_{2P}$17.1 channel subunits, in which one of the two N-glycosylation sites is deactivated (Figure 3G). Mobility shift assays indicate that glycans contribute to ~13% of the molecular mass of mature hK$_{2P}$17.1 ion-channel sub-

units. This fraction is considerably lower than in sodium channels, where posttranslational modifications may cause up to 30% of the molecular mass (Schmidt and Catterall, 1987). In general, membrane glycoproteins may also be modified by O-linked glycosylation. We therefore tested whether this posttranslational modification might be present in hK$_{2P}$17.1 channel subunits. Treatment with O-glycosidase or the antimetabolite O-glycosylation inhibitor BenGal has no detectable effect on protein mobility in SDS gels. Therefore, it seems that O-glycosylation of hK$_{2P}$17.1 channels is not biologically relevant.

It was described that the related ion channel hK$_{2P}$1.1 harbors one glycosylation site located in the P1-M1 interdomain, which was shown by glycosidase treatment and SDS–PAGE (Lesage *et al.*, 1996). The closely related hK$_{2P}$3.1 (TASK-1) and hK$_{2P}$9.1 (TASK-3) channels bear one conserved N-glycan acceptor site located in the P1-M1 interdomain as well. In hK$_{2P}$9.1 channels, deactivation of the N-glycosylation site
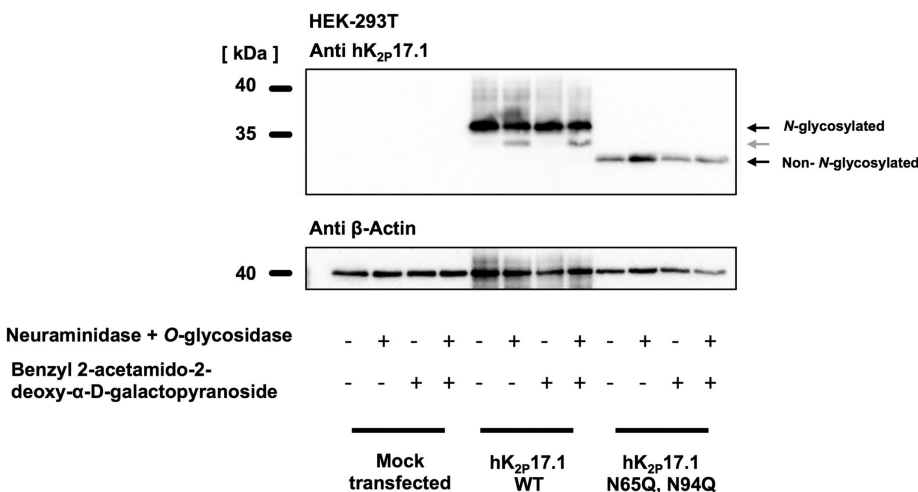
FIGURE 8: In HEK-293 cells, hK$_{2P}$17.1 is not modified by O-glycosylation. Wild-type K$_{2P}$17.1 channels and glutamine mutants lacking N-glycosylation were heterologously expressed in HEK-293T cells. Immunoblots of hK$_{2P}$17.1 after coincubation with the O-glycosylation inhibitor benzyl 2-acetamido-2-deoxy-α-D-galactopyranoside or after treatment of protein lysates with O-glycosidase and neuraminidase are shown. After treatment with O-glycosidase and neuraminidase, a mobility shift can only be observed in N-glycosylated subunits (gray arrow), arguing against O-glycosylation of hK$_{2P}$17.1 channels.

results in reduced membrane expression, whereas their functionality compared with that of unmodified ion channels is not affected (Mant et al., 2013). Mutating glycosylation sites in hK$_{2P}$3.1 channels results in smaller potassium currents than in their WT counterparts, most likely caused by reduced expression at the cell surface (Mant et al., 2013). In contrast to these findings, inserting a proline residue next to the N-glycosylation site of hK$_{2P}$3.1 impaired N-glycosylation without reducing channel currents or transport to the plasma membrane (Goldstein et al., 2016). It remains speculative whether these diverging findings can be attributed to direct effects of the ion-channel mutation or resulted from differences in expression systems used in these studies (Goldstein et al., 2016; Mant et al., 2013). Similarly, hK$_{2P}$18.1 channels exhibit a single functional N-glycosylation. If this site is mutated or N-glycosylation is inhibited, surface expression of hK$_{2P}$18.1 is markedly reduced, resulting in reduced but still measurable outward potassium currents (Egenberger et al., 2010). Another potential N-glycosylation in the P1-M1 interdomain of hK$_{2P}$18.1 that is not conserved in the murine orthologue of K$_{2P}$18.1 displays no functional relevance (Egenberger et al., 2010). Thus, in contrast to hK$_{2P}$17.1 channels, members of the TASK and TRESK subfamilies contain only one glycan acceptor site, and its N-glycosylation seems to be not required for transport to the cell surface. Taken together, these data suggest that N-glycosylation regulates members of the family of K$_{2P}$ channels in a partially different manner. This, however, is not uncommon among ion channels. In case of the HCN ion channel family, N-linked glycosylation is crucial for transport of HCN2 channels to the plasma membrane, while HCN1 channels are markedly less sensitive to deglycosylation (Hegle et al., 2010).

Posttranslational rearrangement and trimming of N-linked glycans results in an extensive diversity, potentiating the complexity of ion channel functions. It is well known that the cellular environment and the metabolic state of the cell have major influence on the quality and quantity of protein glycosylation (Ohtsubo and Marth, 2006). Hence, functional properties of cellular ion-channel composition could be passively and actively controlled via N-glycosylation-mediated regulation of hK$_{2P}$17.1 currents. Further, changes in glycosylation patterns may alter the response to glycan modification via extracellular proteases and sialidases (Lamothe et al., 2018).

Potential limitations
Differences in the quality and quantity of attached glycans have been observed when N-glycosylation in native tissues and after heterologous expression is studied (Shi and Trimmer,1999). To minimize cell line–mediated confounding on hK$_{2P}$17.1 N-glycosylation, X. laevis and two different mammalian cell lines were used in this study.

Clinical implications
Many ion channels undergo N-linked glycosylation, and mutations in glycosylation sites have been identified in potassium channels implicated in long QT syndrome (Petrecca et al., 1999). Congenital disorders of glycosylation are rare autosomal genetic diseases, characterized by genetic defects in glycan synthesis, processing, or targeting (Freeze, 2006). These disorders can affect nearly all organs and are often associated with cardiomyopathies and arrhythmias (Gehrmann et al., 2003). It is likely that altered glycosylation patterns in cardiac ion channels, such as hK$_{2P}$17.1, contribute to the molecular mechanisms of arrhythmogenesis associated with disorders of glycosylation.

Conclusions
In the present study we demonstrate that hK$_{2P}$17.1 channel subunits undergo N-glycosylation. Combining pharmacological, molecular,

and electrophysiological experimental techniques, we show that N-glycosylation of hK$_{2P}$17.1 channels is essential for their transport to the plasma membrane and physiological function.

MATERIALS AND METHODS
Animal studies
This investigation conforms to the guide for the Care and Use of Laboratory Animals (NIH Publication 85-23). All studies involving animals are reported in accordance with the ARRIVE guidelines for reporting experiments involving animals (McGrath et al., 2010). The investigation conforms to Directive 2010/63/EU of the European Parliament. Approval was granted by the local Animal Welfare Committee (reference number G221/12). The authors have taken all steps to minimize the animals' pain and suffering. Surgeries were performed under tricaine anesthesia (1 g/l; pH 7.5). A maximum of three surgeries were performed on each individual frog. After the final taking of oocytes, anaesthetized frogs were killed by decerebration and pithing. The investigators understand the ethical principles under which the journal operates and state that their work complies with its animal ethics checklist.

Molecular biology
Amplification of hK$_{2P}$17.1 from human cerebral cDNA and subcloning in pRAT, an X. laevis and mammalian cell dual purpose expression vector, was described earlier (Gierten et al., 2008). Mutant constructs characterized in this study were generated using the QuickChange Site-Directed Mutagenesis Kit (Stratagene, San Diego, CA). C-terminal myc epitope tags were introduced after removal of the stop codon using standard molecular biology methods as described by Kisselbach et al. (2012) and constructs were subcloned into the X. laevis and mammalian cell dual-purpose expression vector pMax⁺. For chemiluminescence assays, a hemagglutinin (HA)-affinity tag was introduced into the extracellular P2-M4 interdomain as described by Friedreich et al. (2014) via the megaprime PCR technique. Sequences of all plasmid constructs were verified by DNA sequencing (GATC Biotech, Konstanz, Germany). After plasmid linearization, copy RNA was generated by in vitro transcription with a T7 Message Machine Kit (Thermo Fisher Scientific, Waltham, MA). Integrity of RNA transcripts was confirmed by agarose gel electrophoresis and RNA concentrations were determined using Nanodrop spectrophotometry (ND-1000; peqLab Biotechnology GmbH, Erlangen, Germany).

Cell culture
Human embryonic kidney cells (HEK-293T) and HeLa cells were cultured in DMEM (Thermo Fisher Scientific) supplemented with 10% fetal calf serum (Thermo Fisher Scientific), 100 U/l penicillin G sodium, and 100 µg/ml streptomycin sulfate. Cells were kept under 95% humidified air and 5% CO$_2$ at 37°C. For immunofluorescence, cells were seeded on glass coverslips before transient transfection with Lipofectamin 3000 (Thermo Fisher Scientific) following the manufacturer's instructions. Protein expression for protein biochemistry was performed by treating 80% confluent T75 tissue culture flasks (Sarstedt, Nümbrecht, Germany) with a mixture of 635 µl ddH$_2$O, 815 µl 300 mM NaCl, 180 µl polyethylenimine solution (0.323 g/l; Polysciences, Warrington, PA), and 22 µg of plasmid DNA. The O-glycosylation blocker benzyl-2-acetamido-2-deoxy-α-$_D$-galactopyranoside (BenGal) and the N-glycosylation inhibitor tunicamycin (Sigma Aldrich, St. Louis, MO) were dissolved in DMSO to stock solutions of 1 mg/ml and 300 mM, respectively, and stored at –20°C. Indicated cell culture media were supplemented with 1 µg/ml tunicamycin, 300 µM BenGal, or equal amounts of DMSO.

Oocyte preparation

Oocytes were isolated from *X. laevis* (Xenopus Express, Vernassal, France) ovarian lobes after surgical extirpation under tricaine anesthesia (1 g/l; pH 7.5). Oocyte collection was alternated between left and right ovaries. A maximum of three surgeries were performed on each individual frog. Following collagenase treatment, defolliculated stage V–VI oocytes were manually selected under a stereomicroscope (STEMI 2000; Zeiss, Oberkochen, Germany) and maintained in a standard oocyte solution (SOS), consisting of 100 mM NaCl, 2 mM KCl, 1.8 mM CaCl$_2$, 1 mM MgCl$_2$, 5 mM HEPES, 2.5 mM pyruvate, and 100 µg/ml gentamicin (pH 7.6). Copy RNA (cRNA; 12.5–25 ng in 46 nl per oocyte) was injected using the Nanoject system (Drummond Scientific Company, Broomall, PA). Where indicated, oocytes were either coinjected with 2 ng tunicamycin per cell or incubated in media containing 0.03–3 µg/ml tunicamycin to inhibit N-glycosylation. Respective controls were performed by incubation or injecting equal amounts of DMSO.

Protein preparation and Western blot

Homogenization of *X. laevis* oocytes was performed 36 h after injection, using a glass–Teflon tissue homogenizer. Proteins were solubilized for 1 h at 4°C in oocyte lysis buffer (100 mM NaCl, 40 mM KCl, 20 mM HEPES, 1 mM EDTA, 10% glycerol, and 1% 3-[{3-cholamidopropyl}dimethylammonio]-1-propanesulfonate hydrate [CHAPS]; pH 7.4). The supernatant was clarified by repeated centrifugations at 5000 × *g* (5 min) followed by a final centrifugation at 15,000 × *g* (20 min). HEK-293T cells were harvested 36 h after transfection by scraping on ice. Samples were subjected to cell lysis in radioimmunoprecipitation (RIPA) buffer (150 mM NaCl, 20 mM Tris-HCl, 1 mM EDTA, 0.5% NP-40, 0.5% sodium deoxycholate, 1 mM NaF, 1 mM Na$_3$VO$_4$), agitated for 30 min at 4°C, and clarified by centrifugation at 15,000 × *g* for 30 min at 4°C. All buffer solutions used for protein preparation were supplemented with cOmplete mini protease inhibitor cocktail (Roche Diagnostics, Mannheim, Germany). Protein concentration was determined using the bicinchoninic acid (BCA) protein assay (Thermo Fisher Scientific). Where indicated, glycosidase digest with PNGase F or neuraminidase and O-glycosidase (New England Biolabs, Ipswich, MA) was performed according to the manufacturer's instructions. Protein samples were mixed with Laemmli sample buffer (Biorad, Hercules, CA), supplemented with 150 mM dithiothreitol (DTT) and 5% β-mercaptoethanol, boiled for 5 min at 95°C, and subjected to SDS–PAGE on 10% Tris-HCl gels as described earlier (Schmidt *et al.*, 2015). Where indicated treatment with DTT and β-mercaptoethanol was omitted. After wet transfer to polyvinylidenfluoride membranes, immunodetection was performed using the following primary antibodies: ab198043 (Abcam, Cambridge, UK), polyclonal rabbit anti-hK$_{2P}$17.1 (1:300); sc-390435 (Santa Cruz Biotechnology, Heidelberg, Germany); monoclonal mouse anti-hK$_{2P}$17.1 (1:100); sc-47778 (Santa Cruz Biotechnology); mouse monoclonal anti-β-actin (1:1000); G8140-11 (US Biological, Swampscott, MA) mouse monoclonal anti-GAPDH (1:10,000) and sc-789 (Santa Cruz Biotechnology) polyclonal rabbit anti–c-myc (1:50), as well as appropriate horseradish peroxidase (HRP)-conjugated secondary antibodies: NAV934 (GE Healthcare, Chicago, IL) donkey anti-rabbit (1:3000) and sc-2005 (Santa Cruz Biotechnology) goat anti-mouse (1:3000). Signals were developed using the enhanced chemiluminescence assay (GE Healthcare) and quantified using a FluorChem Q luminescence detector (Cell BioSciences, Palo Alto, CA).

Chemiluminescence assay

For quantification of cell surface expression, hK$_{2P}$17.1 constructs harboring an extracellular HA tag were expressed in Xenopus oocytes. Cells were incubated for 30 min at 4°C in standard oocyte-maintaining solution (SOS) containing 1% bovine serum albumin (BSA) to block nonspecific binding of antibodies. Labeling was performed with monoclonal rat anti-HA antibody (clone 3F10, Roche; 1 mg/ml) in 1% BSA/SOS for 60 min at 4°C. After repeated washing steps, cells were incubated with peroxidase-conjugated goat anti-rat secondary antibody (AP136P, Sigma Aldrich, 1:10,000) diluted in 1% BSA/SOS for 60 min at 4°C. Oocytes were washed thoroughly for 60 min at 4°C in SOS without BSA and placed in Amersham ECL-Prime Western blotting detection reagent (GE Healthcare). Chemiluminescence was detected by a FluorChem Q luminescence detector (Cell BioSciences) and quantified using ImageJ software version 1.51f (Schneider *et al.*, 2012). Uninjected oocytes served as negative controls.

HEK-293T surface biotinylation assay

Biotinylation of lysine-exposing surface proteins was performed 36 h after transient transfection by incubation with 0.5 mg/ml cell-impermeable, noncleavable sulfo-NHS-SS-Biotin (Pierce, Rockford, IL) for 30 min at 4°C. Unbound biotin reagent was quenched three times with 4 ml glycine (10 mM) in PBS (pH 8.0). After homogenization, proteins were solubilized as described. Biotin-labeled proteins were isolated from protein samples by incubation with streptavidin beads (Pierce) for 2 h at 4°C. Following repeated washing, surface proteins were liberated by boiling for 5 min in DTT and β-mercaptoethanol-containing Laemmli sample buffer.

Fluorescence imaging

At 36 h after transient transfection, HeLa cells were washed with phosphate-buffered saline (PBS) and fixed with 4% paraformaldehyde for 15 min. Following incubation with PBS/Alexa Fluor 594-coupled wheat germ agglutinin (WGA), 3 µg/ml (W11262, Thermo Fisher Scientific), cells were washed in PBS and incubated with permeabilization and blocking buffer consisting of PBS/1% BSA/0.5% Triton X-100/10% normal goat serum (Santa Cruz Biotechnology) for 30 min at 4°C. For immunolabeling, cells were incubated for 2 h at 4°C with monoclonal mouse anti-hK$_{2P}$17.1 (1:100, sc-47778, Santa Cruz Biotechnology) in PBS with 1% BSA, 0.5% Triton X-100, and 3% normal goat serum. Alexa Fluor 488-coupled polyclonal goat anti-mouse secondary antibodies (A-11001, Thermo Fisher Scientific) were used at a dilution of 1:1000 in the same buffer. After repeated washing, coverslips were mounted with FluorSave (Merck Chemicals GmbH, Darmstadt, Germany) antifade solution and examined using an Olympus IX51 microscope.

Electrophysiology

Two-electrode voltage clamp (TEVC) recordings from *Xenopus* oocytes were performed 1–3 d after cRNA injection as described (Wiedmann *et al.*, 2018). Whole cell currents were measured with an OC-725C amplifier (Warner Instruments, Hamden, CT) using pCLAMP9 software (Axon Instruments, Foster City, CA) for data acquisition and analysis. The standard extracellular solution contained 96 mM NaCl, 4 mM KCl, 1.1 mM CaCl$_2$, 1 mM MgCl$_2$, 5 mM 4-(2-hydroxyethyl)-1-piperazineethanesulfonic acid (HEPES), pH 8.5. Microelectrodes fabricated from glass pipettes (GB 100F-10, Science Products, Hofheim, Germany) using a Flaming/Brown P-87 micropipette puller (Sutter Instruments, Novato, CA) were backfilled with 3 M KCl, yielding resistances ranging from 0.5 to 1.5 MΩ. All experiments were carried out at room temperature (20–22°C). Holding potentials were –80 mV in all experiments, and leak currents were not subtracted. Vernakalant was purchased from Merck Sharp

& Dohme (Haar, Germany) and stored in 1 ml aliquots (51.8 mM) at –20°C.

Data analysis, homology model, and statistics

We applied the bioinformatic prediction software NetNGlyc 1.0 server (www.cbs.dtu.dk/services/NetNGlyc/). The prediction tool suggested asparagine residues 65 and 94 as potential N-glycan acceptors with probability scores of 0.72 and 0.73. Multiple sequence alignment was performed with the Clustal Omega algorithm (Sievers *et al.*, 2011). Three-dimensional open state structure models of hK$_{2P}$17.1 channels were calculated using the SWISS-MODEL platform (Arnold *et al.*, 2006; Guex *et al.*, 2009; Kiefer *et al.*, 2009; Biasini *et al.*, 2014). Data are presented as mean ± standard error of the mean (SEM). PCLAMP 9 (Axon Instruments, Foster City, CA) and Prism 5 (GraphPad Software, La Jolla, CA) software was used for data acquisition and statistical analysis. Student's t tests (two-tailed tests) were applied to assess statistical significance. A p value <0.05 was considered statistically significant. If the hypothesis of equal means could be rejected at the 0.05 level, pairwise comparisons of groups were made and the probability values were adjusted for multiple comparisons using the Bonferroni correction.

REFERENCES

Arnold K, Bordoli L, Kopp J, Schwede T (2006). The SWISS-MODEL Workspace: a web-based environment for protein structure homology modelling. Bioinformatics 22, 195–201.

Baycin-Hizal D, Gottschalk A, Jacobson E, Mai S, Wolozny D, Zhang H, Krag SS, Betenbaugh MJ (2014). Physiologic and pathophysiologic consequences of altered sialylation and glycosylation on ion channel function. Biochem Biophys Res Commun 453, 243–253.

Biasini M, Bienert S, Waterhouse A, Arnold K, Studer G, Schmidt T, Kiefer F, Cassarino TG, Bertoni M, Bordoli L, Schwede T (2014). SWISS-MODEL: modelling protein tertiary and quaternary structure using evolutionary information. Nucleic Acids Research 42, W252–W258.

Brohawn SG, del Mármol J, MacKinnon R (2012). Crystal structure of the human K$_{2P}$ TRAAK, a lipid- and mechano-sensitive K$^+$ ion channel. Science 335, 436–441.

Chai S, Wan X, Ramirez-Navarro A, Tesar PJ, Kaufman ES, Ficker E, George AL, Deschênes I (2018). Physiological genomics identifies genetic modifiers of long QT syndrome type 2 severity. J Clin Invest 128, 1043–1056.

Decher N, Maier M, Dittrich W, Gassenhuber J, Brüggemann A, Busch AE, Steinmeyer K (2001). Characterization of TASK-4, a novel member of the pH-sensitive, two-pore domain potassium channel family. FEBS Lett 492, 84–89.

Domingues-Montanari S, Fernández-Cadenas I, Del Río-Espinola A, Mendioroz M, Fernandez-Morales J, Corbeto N, Delgado P, Ribó M, Rubiera M, Obach V, *et al.* (2010). KCNK17 genetic variants in ischemic stroke. Atherosclerosis 208, 203–209.

Egenberger B, Polleichtner G, Wischmeyer E, Döring F (2010). N-linked glycosylation determines cell surface expression of two-pore-domain K$^+$ channel TRESK. Biochem Biophys Res Commun 391, 1262–1267.

Enyedi P, Czirják G (2010). Molecular background of leak K$^+$ currents: two-pore domain potassium channels. Physiol Rev 90, 559–605.

Feliciangeli S, Chatelain FC, Bichet D, Lesage F (2015). The family of K$_{2P}$ channels: salient structural and functional properties. J Physiol 593, 2587–2603.

Freeman LC, Lippold JJ, Mitchell KE (2000). Glycosylation influences gating and pH sensitivity of I(sK). J Membr Biol 177, 65–79.

Freeze HH (2006). Genetic defects in the human glycome. Nat Rev Genet 7, 537–551.

Friedrich C, Rinné S, Zumhagen S, Kiper AK, Silbernagel N, Netter MF, Stallmeyer B, Schulze-Bahr E, Decher N (2014). Gain-of-function mutation in TASK-4 channels and severe cardiac conduction disorder. EMBO Mol Med 6, 937–951.

Gehrmann J, Sohlbach K, Linnebank M, Böhles HJ, Buderus S, Kehl HG, Vogt J, Harms E, Marquardt T (2003). Cardiomyopathy in congenital disorders of glycosylation. Cardiol Young 13, 345–351.

Gierten J, Ficker E, Bloehs R, Schlömer K, Kathöfer S, Scholz E, Zitron E, Kiesecker C, Bauer A, Becker R, *et al.* (2008). Regulation of two-pore-domain (K$_{2P}$) potassium leak channels by the tyrosine kinase inhibitor genistein. Br J Pharmacol 154, 1680–1690.

Goldstein M, Rinné S, Kiper AK, Ramírez D, Netter MF, Bustos D, Ortiz-Bonnin B, González W, Decher N (2016). Functional mutagenesis screens reveal the 'cap structure´ formation in disulfide-bridge free TASK channels. Sci Rep 6, 19492.

Goldstein SAN, Bockenhauer D, O'Kelly I, Zilberberg N (2001). Potassium leak channels and the KCNK family two-P-domain subunits. Nat Rev Neurosci 2, 175–184.

Guex N, Peitsch MC, Schwede T (2009). Automated comparative protein structure modeling with SWISS-MODEL and Swiss-PdbViewer: a historical perspective. Electrophoresis 30, S162–S173.

He J, Xu J, Castleberry AM, Lau AG, Hall RA (2002). Glycosylation of beta(1)-adrenergic receptors regulates receptor surface expression and dimerization. Biochem Biophys Res Commun 297, 565–572.

He L, Ma Q, Wang Y, Liu X, Yuan Y, Zhang Y, Ou W, Liu L, Tan X, Wang X (2014). Association of variants in KCNK17 gene with ischemic stroke and cerebral hemorrhage in a Chinese population. J Stroke Cerebrovasc Dis 23, 2322–2327.

Hegle AO, Nazzari H, Roth A, Angoli D, Accilli EA (2010). Evolutionary emergence of N-glycosylation as a variable promoter of HCN channel surface expression. Am J Physiol Cell Physiol 298, C1066–C1076.

Ketchum KA, Joiner WJ, Sellers AJ, Kaczmarek LK, Goldstein SA (1995). A new family of outwardly rectifying potassium channel proteins with two pore domains in tandem. Nature 376, 690–695.

Khanna R, Myers MP, Lainé M, Papazian DM (2001). Glycosylation increases potassium channel stability and surface expression in mammalian cells. J Biol Chem 276, 34028–34034.

Kiefer F, Arnold K, Künzli M, Bordoli L, Schwede T (2009). The SWISS-MODEL Repository and associated resources. Nucleic Acids Res 37, D387–D392.

Kisselbach J, Schweizer PA, Gerstberger R, Becker R, Katus HA, Thomas D (2012). Enhancement of K$_{2P}$2.1 (TREK1) background currents expressed in *Xenopus* oocytes by voltage-gated K$^+$ channel β subunits. Life Sci 91, 377–383.

Kuo SC, Lampen, JO (1974). Tunicamycin—an inhibitor of yeast glycoprotein synthesis. Biochem Biophys Res Commun 58, 287–295.

Lamothe SM, Hulbert M, Guo J, Li W, Yang T, Zhang S (2018). Glycosylation stabilizes hERG channels on the plasma membrane by decreasing proteolytic susceptibility. FASEB J 5, fj201700832R.

Lesage F, Guillemare E, Fink M, Duprat F, Lazdunski M, Romey G, Barhanin J (1996). TWIK-1, a ubiquitous human weakly inward rectifying K$^+$ channel with a novel structure. EMBO J 15, 1004–1011.

Ma Q, Wang Y, Shen Y, Liu X, Zhu X, Zhang H, Liu L, Tan X, Wang L, Wang X (2013). The rs10947803 SNP of KCNK17 is associated with cerebral hemorrhage but not ischemic stroke in a Chinese population. Neurosci Lett 539, 82–85.

Mant A, Williams S, Roncoroni L, Lowry E, Johnson D, O'Kelly I (2013). N-glycosylation-dependent control of functional expression of background potassium channels K$_{2P}$3.1 and K$_{2P}$9.1. J Biol Chem 288, 3251–3264.

McGrath J, Drummond G, Kilkenny C, Wainwright C (2010). Guidelines for reporting experiments involving animals: the ARRIVE guidelines. Br J Pharmacol 160, 1573–1576.

Miller AN, Long SB (2012). Crystal structure of the human two-pore domain potassium channel K$_{2P}$1. Science 335, 432–436.

Ohtsubo K, Marth JD (2006). Glycosylation in cellular mechanisms of health and disease. Cell 126, 855–867.

Petrecca K, Atanasiu R, Akhavan A, Shrier A (1999). *N*-linked glycosylation sites determine HERG channel surface membrane expression. J Physiol 515, 41–48.

Schmidt C, Wiedmann F, Voigt N, Zhou XB, Heijman J, Lang S, Albert V, Kallenberger S, Ruhparwar A, Szabó G, *et al.* (2015) Upregulation of $K_{2P}3.1$ K^+ current causes action potential shortening in patients with chronic atrial fibrillation. Circulation 132, 82–92.

Schmidt C, Wiedmann F, Zhou XB, Heijman J, Voigt N, Ratte A, Lang S, Kallenberger SM, Campana C, Weymann A, *et al.* (2017). Inverse remodelling of $K_{2P}3.1$ K^+ channel expression and action potential duration in left ventricular dysfunction and atrial fibrillation: implications for patient-specific antiarrhythmic drug therapy. Eur Heart J 38, 1764–1774.

Schmidt JW, Catterall WA (1987). Palmitylation, sulfation, and glycosylation of the alpha subunit of the sodium channel. Role of post-translational modifications in channel assembly. J Biol Chem 262, 13713–13723.

Schneider CA, Rasband WS, Eliceiri KW (2012). NIH Image to ImageJ: 25 years of image analysis. Nat Methods 9, 671–675.

Seyler C, Schweizer PA, Zitron E, Katus HA, Thomas D (2014). Vernakalant activates human cardiac K2P17.1 background K+ channels. Bioch Biophys Res Comm 451, 415–420.

Shi G, Trimmer JS (1999). Differential asparagine-linked glycosylation of voltage-gated K^+ channels in mammalian brain and in transfected cells. J Membr Biol 168, 265–273.

Sievers F, Wilm A, Dineen DG, Gibson TJ, Karplus K, Li W, Lopez R, McWilliam H, Remmert M, Söding J, *et al.* (2011). Fast, scalable generation of high-quality protein multiple sequence alignments using Clustal Omega. Mol Syst Biol 7, 539.

Tarentino AL, Gómez CM, Plummer TH (1985). Deglycosylation of asparagine-linked glycans by peptide: N-glycosidase F. Biochemistry 24, 4665–4671.

Thornhill WB, Wu MB, Jiang X, Wu X, Morgan PT, Margiotta JF (1996). Expression of Kv1.1 delayed rectifier potassium channels in Lec mutant Chinese hamster ovary cell lines reveals a role for sialidation in channel function. J Biol Chem 271, 19093–19098.

Wiedmann F, Schmidt C, Lugenbiel P, Staudacher I, Rahm AK, Seyler C, Schweizer PA, Katus HA, Thomas D (2016). Therapeutic targeting of two-pore-domain potassium (K_{2P}) channels in the cardiovascular system. Clin Sci (Lond) 130, 643–650.

Wiedmann F, Schulte JS, Gomes B, Zafeiriou MP, Ratte A, Rathjens F, Fehrmann E, Scholz B, Voigt N, Müller FU, *et al.* (2018). Atrial fibrillation and heart failure-associated remodeling of two-pore-domain potassium (K_{2P}) channels in murine disease models: focus on TASK-1. Basic Res Cardiol 113, 27.